arXiv:cond-mat/0408324v1 [cond-mat.mtrl-sci] 13 Aug 2004

Finite lattice size effect in the ground state phase diagram of quasi-two-dimensional magnetic dipolar dots array with perpendicular anisotropy

R. H. He[1], X. F. Jin[1]*
[1] *Applied Surface Physics Laboratory, Physics Department, Fudan University, Shanghai 200433, China*
(Dated: March 22, 2022)

A prototype Hamiltonian for the generic patterned magnetic structures, of dipolar interaction with perpendicular anisotropy, is investigated within the finite-size framework by Landau-Lifshift-Gilbert classical spin dynamics. Modifications on the ground state phase diagram are discussed with an emphasis on the disappearance of continuous degeneracy in the ground state of in-plane phase due to the finite lattice size effect. The symmetry-governed ground state evolution upon the lattice size increase provides a critical insight into the systematic transition to the infinite extreme.

PACS numbers: 75.50.Ee, 75.25.1z, 75.30.2m, 75.70.Kw

Nanoscale magnetism of patterned magnetic structures (PDS) has aroused a great deal of research interest due to its potential technological applications[1] in high-density magnetic storage media and spintronic devices such as magnetic random access memory. Recent lithographic technologies have rendered possible the design of various geometry of the quasi-two-dimensional(2D) uniform array composed of identical elements with a well-defined composition, shape and size in sub-micrometer scale[2] and hence the control of magnetic properties of the system. Each small-size dot, made up of a large number of spins which interact ferromagnetically through the intradot exchange interaction, tends to be kept in a single-domain acting as a giant spin in response to the exerted magnetic field[2]. As a contrast, the interdot exchange interaction term is completely precluded from the generic Hamiltonian in describing such an interacting dipole system[3] because of the large interdot spacing,

$$H_{int} = -D\sum_i S_z^2 + U_{dipole}, \tag{0.1}$$

$$U_{dipole} = \frac{1}{2}\sum_{i,j}\Omega[\frac{1}{r_{ij}^3}(\vec{S}_i\cdot\vec{S}_j) - \frac{3}{r_{ij}^5}(\vec{r}_{ij}\cdot\vec{S}_i)(\vec{r}_{ij}\cdot\vec{S}_j)], \tag{0.2}$$

where D represents the on-site effective anisotropy strength, which is the joint contributions by magnetocrystalline anisotropy and shape anisotropy resulted from intradot dipolar coupling, U_{dipole} the interdot dipolar interaction[4], $\vec{S}_{i(j)}$ is the giant spin at site $i(j)$, equal to the total moment of spins inside, $\vec{r}_{ij}$ the vector connecting the two sites.

In recent years, driven by the efforts in resolving complex micromagnetic mechanisms for, such as spin reorientation transition[5] and anti-ferromagnetic domain nucleation[6], as well as the growing extensive interest in understanding the magnetism-related problems found in various kinds of novel material whose interspin spacing is relatively large in the atomic scale, such as high-spin molecular[7, 8] and some high-temperature superconductors with magnetic irons forming a quasi-2D plane[9], considerable theoretical attentions and experimental efforts are put into the understanding of the dominating dipolar effect involved in the prototype Hamiltonian.

Theoretically, however, as the uniqueness of PDS, the finite-size nature, is seldom emphasized. Most analytical works based on infinite dipole sums[10] as well as numerical works using a period boundary condition (PBC)[5, 9, 11](***more to be cited here***) do not practically apply to the PDS. Previous results on the phase diagram of the easy-axis dipolar Hamiltonian are expected to be adjusted, in the framework where a realistic truncation on the dipole sums or the free boundary condition (FBC) is used, before a direct comparison of with experiments on PDS can be made[5, 9]. On the other hand, experimentally, efforts spent on the PDS are expected to be rewarding in that they provide a rather handy way in finetuning the relative strength of different interactions by only changing the definable geometrical parameters of the system while keeping the matrix material unchanged, and hence facilitates an easy probe by the mature spacially-averaged measurements or spacially-resolved imaging techniques[3] into a wide range of phase diagram of the system, which in turn serves the general understanding of the dipolar physics as long as the precursory knowledge in the role of finite size is available.

In this paper, we attempt to build up the missing link in between by presenting a systematic size-dependent evolution of the ground state phase diagram of the easy-axis dipolar Hamiltonian. In contrast to the robustness of the out-of-plane (OOP) phase, the in-plane (IP) phase exhibits a pronounced modification under the finite-size influence. The difference of the detailed dynamics of the evolution as function of lateral size (L) for lattices with an even and odd number L, is explained from the symmetry point of view. The even-odd symmetry difference as well as the in-plane anisotropic content of dipolar interaction on 2D lattice tend to be concealed by its long-range nature upon $L \to \infty$, as suggested by the extreme picture

*Electronic address: xfjin@fudan.ac.cn

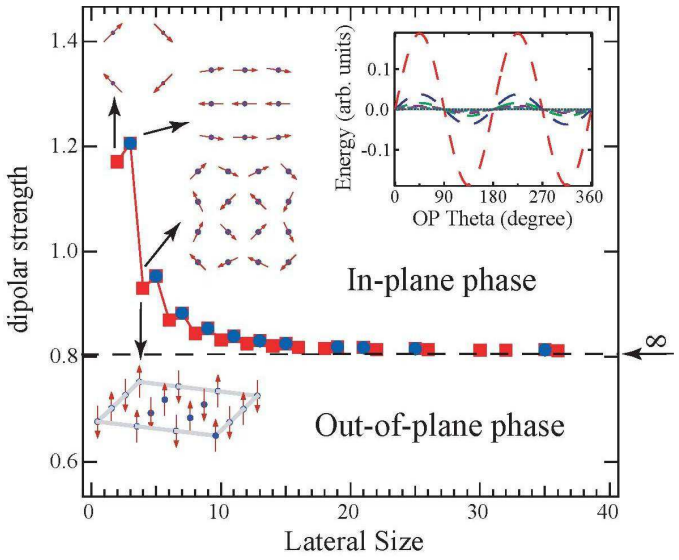


FIG. 1: (color) The finite-size phase diagram of the easy-axis dipolar Hamiltonian. The zigzag boundary separates the in-plane phase (the upper half) from the out-of-plane phase (the lower half). Insets in the in-plane phase: the ground state spin configurations for $L = 2, 3, 4$, respectively, and the OP theta-dependent in-plane AFM state energy for $L = 2, 4, 6, 8, 10, 14, 32$ (dash lines with decreasing length) and all odd L's (grey based line); the inset in the out-of-plane phase: the out-of-plane AFM state spin configuration (3D) at $L = 4$.

finally given.

Landau-Lifshift-Gilbert classical spin dynamics is strictly followed to investigate the physical ground state and dynamical properties of the system under zero field[6]. For clarity, the module of spin vector, the anisotropy strength, the gyromagnetic constant (as the unit reference for time and effective field strength), and damping coefficient are set to unity unless specified otherwise. Predictor-corrector method with Runge-Kutta initialization is used to maintain a high accuracy of the numerical integration of equation of motion[13], which is required for the realistic comparison between our results with experiments as well as true dynamics starting from a given initial spin configuration. The investigation of finite lattice size effect demands a differentiation on the free boundary condition (FBC) and periodic boundary condition (PBC). Different from the only use of PBC in MC simulation which always serves to approach the infinite system with a well-defined temperature in the statistical sense, our spin dynamics simulations are carried out using FBC for the finite-size lattices and PBC for the infinite one.

In Fig. 1, we recap the the phase diagram of the easy-axis dipolar Hamiltonian with its finite-size modifications. For the infinite lattice, an out-of-plane (OOP) phase lies in the small dipolar strength (DD) regime, whose ground state is characterized by an OOP order parameter, $\vec{M}_z = \frac{1}{N}\sum_i (-1)^{m+n} S^z$ (OOP-AFM), where m and n are row and column index for the square lattice, respectively; the planar nature of the 2D dipolar Hamiltonian recovers by yielding an in-plane (IP) phase upon DD increase, with its continuously degenerate ground state described by the IP order parameter (OP) $\vec{M}_{xy} = \frac{1}{N}\sum_i [(-1)^n S^x \hat{x} + (-1)^m S^y \hat{y}]$ (IP-AFM, $|\vec{M}_{xy}|$ the OP module $|OP|$, $\arctan(\frac{M_y}{M_x})$ the OP theta). In the OOP phase, when lattice size reduces to finite, the OOP-AFM state (inset of Fig. 1) remains stable regardless of any specific lateral size (L). Exhaustive simulations (up to $L = 128$, 100 1000 per L, $DD = 0.5$) starting from random initial configurations show this state has the lowest energy. The robustness of the out-of-plane ground state points to the persistence of 2D AFM Ising nature (due to the disappearance of the second term in dipolar interaction) upon finite truncation in the dipole sum[10]. As a contrast, a partial recovery of the effective in-plane anisotropy at the cost of the long-range nature of dipolar Hamiltonian removes largely the ground state degeneracy in the in-plane phase. As shown in the inset of Fig. 1, for the even L's, the IP-AFM states are no longer continuously degenerate, whose energies exhibit a sine distribution as a function of the OP theta with a rapidly decreasing amplitude as L increases; for all odd L's, interestingly, there is no difference in energy for these IP-AFM states.

Notably, as for the IP-AFM states, the OP symmetry is different for the even- and odd-L lattices, which can be investigated based on symmetry operations on the spin lattice. The axial OP symmetry for the even-L lattice is $\pm 45°$ while $\pm 45°$ as well as $0°$ and $90°$ for the odd-L lattice[14]. Bearing this in mind, we conduct a further examination on the stability of the IP-AFM states at various L's by independent spin dynamics simulations taking them as the initial states and, similar as in the OOP phase case, the ground state at each L is confirmed by simulations starting from random initial spin configurations. As illustrated in the insets of Fig. 1), the only ground state of $L = 2$ is the IP-AFM state with the $135°$ OP theta (denoted as OP135, and similarly hereafter), which can be regarded as a fully boundary-distorted (BD) spin configuration. When $L > 2$, the boundary effect is weakened as the number ratio between the inside spins and the boundary spins increases. As seen in the insets, the ground states of $L = 3, 4$ have clearly hybrid compositions, whose central regions basically maintain the original spin alignments while the peripheral spins tends to align along the borders, and are denoted as BD-OP0 and BD-OP135, respectively.

A prominent feature of the L-dependent phase boundary, which is determined from the comparison in energy between the OOP and IP ground states as a function of DD for each L, is its zigzag (oscillatory) decrease asymptotically to the value of infinite lattice. The shrinkage of the out-of-plane phase upon L increase is the result of the long-range nature of the dipolar interaction which favors in-plane magnetization; the non-monotonous behavior, one of the characteristics of finite size effects frequently encountered in other nanosciences[15], not only suggests

the AFM nature of the dipolar ground state, but also contains critical information about the dynamical evolution of the system as it extends to infinite by following its unique OP symmetry different for the even-L case and the odd one.

In order to have a quantitative insight into the dynamical evolution, we continue to use the OP expression on states during the relaxation from the given initial states ($|OP| = 1$) though their effective $|OP|$'s are expected to reduce dependent on the OP inhomogeneity. A prototype of the $|OP|$ evolution is shown in Fig. 2(b), which is characterized by a preceding rapid drop and a slow saturation. The boundary relaxation proceeds with a major minimization on the total energy and ends up with a BD state of the lowest $|OP|$, whose spin configuration is exemplified in Fig. 2(c) for OP67.5. The subsequent relaxation mainly involves the rotation of OP to reach finally a certain meta-stable state. The whole physical path is illustrated in the inset of Fig. 2(a) for initial states with different OP theta values ($L = 10$). Notably, besides the ground state BD-OP135, a meta-stable state, BD-OP45, forms at $L = 6$ by attracting the initial states with OP theta in its proximity. For example, in Fig. 2(a), the OP22.5 state, which is attracted to the BD-OP315 at $L = 2, 4$, experiences a pronounced transformation in its physical path leading to a different final state, BD-OP45, at $L > 6$.

To obtain a systematic clarification, we simulate in Fig.

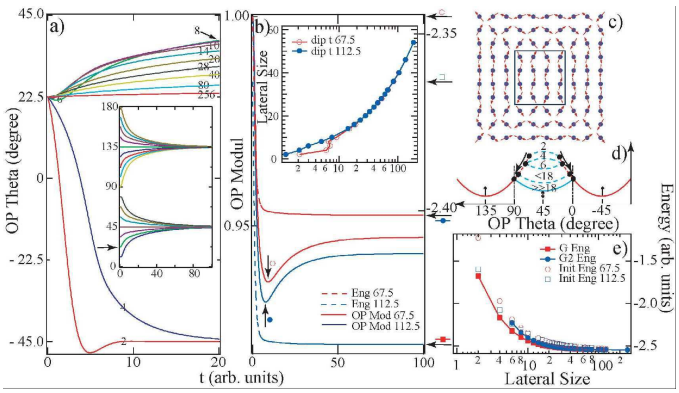


FIG. 2: (color) Spin dynamics for the even-L lattices. (a) L-dependent evolution of the OP22.5 state (L indicated on curves). Inset: typical evolutions of various OP theta states at intermediate L ($L = 10$). (b) typical evolutions in unit energy and $|OP|$ of OP67.5 and OP112.5 states at intermediate L ($L = 10$). The L-dependent relaxation time positions (semilog) of the dips in the two $|OP|$ curves are summarized in the inset. (c) the spin configuration ($L = 10$) corresponding to the dip in the $|OP|$ curve of OP67.5, namely BD-OP67.5 in the text. Note that spins in the framed region are basically free from the boundary distortion. (d) schematics showing the evolution of 3D free energy surface in the transverse view. Numbers are L values and arrows indicate the relative motion of energy surface. (e) the L-dependent energies of the ground state BD-OP135, the metastable state BD-OP45 and the initial states OP67.5 and OP112.5 (semilog).

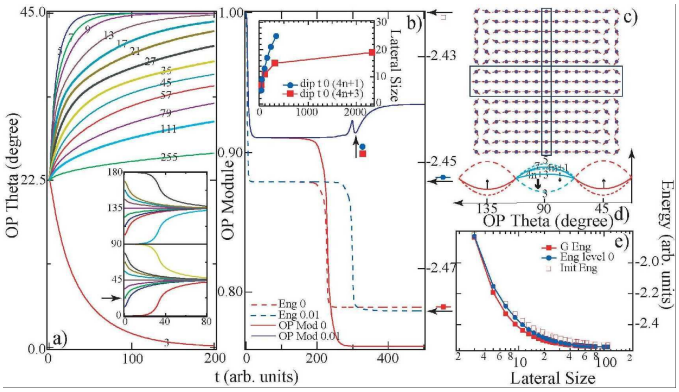


FIG. 3: (color) Spin dynamics for the odd-L lattices. (a) L-dependent evolution of the OP22.5 state (L indicated on curves). Inset: typical evolutions of various OP theta states at intermediate L ($L = 9$). (b) evolutions in unit energy and OP module of OP0 and OP0.01 states ($L = 10$). The L-dependent relaxation time position of the dip in the OP module curve of OP0.01 is summarized in the inset. (c) the spin configuration ($L = 15$) corresponding to the level in the OP module curve of OP0 (OP0.01), namely the intermediate BD-OP0 in the text. Note that a row dislocation and a column dislocation are as framed respectively. (d) schematics showing the evolution of 3D free energy surface in the transverse view. Numbers are L values and arrows indicate the relative motion of energy surface. (e) the L-dependent energies of the ground state BD-OP45, the intermediate BD-OP0 and the initial state OP theta (theta any) (semilog).

2(d) the transverse view of the imaginary free energy surface[16], which facilitates our understanding of the OP rotation process following the boundary-distortion. The convex free energy surface centering at OP theta 45° is depressed upon L increase until its substitution by a concave at $L = 6$. The two concaves at OP theta 45° and 135° intercepts to form a watershed somewhere in between, which is kept pushing asymptotically toward OP theta 90° by the further lowering in energy of the OP theta 45° concave and meanwhile enlarging its attraction area. The proximity of the watershed induces some seemingly odd features in dynamics of, for example, the OP22.5 at $L = 6$ (Fig. 2(a)). As summarized in the inset of Fig. 2(b), there exists a pronounced difference in boundary relaxation time for the two initial states located symmetrically about OP theta 90°, which tends to diminish as L increases up to 18. This difference in time suggests the difference in physical relaxation path taken respectively by the two initially symmetric states. The latter is governed by the difference in topology of the free energy surface due to the joint effect of the asymmetry in initial state energy about OP90, which almost disappears at $L > 16$ (Fig. 2(e)), and the asymmetry by a finite displacement in OP theta position of the watershed from 90°. The 90°-axis OP symmetry recovery can also be evidenced by the disappearance of the initial inequality in the final-state $|OP|$ between BD-OP135 and BD-OP45 at roughly the same L (Fig. 4(a)). From $L = 18$, the further modification on the free energy surface topology

occurs mainly along the energy axis (vertically). As indicated by Fig. 2(e), a gradual loss of the transverse gradient precedes the final loss of longitudinal gradient. The former is achieved by the flattening of both concaves at the same time with the fully recovery of symmetry about 45°-axis by a vertical alignment of the bottoms of both concaves; the latter is expected when the initial and final states converge in energy, which tends to flatten the OP theta evolution curves (Fig. 2(a)) and drives the boundary relaxation time to be infinite (the inset of Fig. 2(b)).

A similar outline is found for the story in the odd-L case though the details are different due to its difference in OP symmetry. The free energy surface has an opposite topology between $L = 3$ and 5. The transformation in the OP theta evolution of OP22.5 in Fig. 3(a) shows the appearance of a new meta-stable state, BD-OP45. This only ground state for $L > 3$ takes over all the initial states, except the exact OP0 (inset of Fig. 3(a)). Accordingly, in the $|OP|$ evolution, apart from the BD states found corresponding to the module minimum as in the even-L case, there exists an intermediate flat region for the OP0 initial states before the final arrival of a fully BD-OP0 state, which is metastable with a slightly higher energy and a much reduced $|OP|$ than the ground state BD-OP45 (Fig. 3(b)). A small deviation on the initial-state OP theta from 0° (OP0.01, in Fig. 3(b)) leads to an ultimate fall onto BD-OP45 after a substantial stay in the intermediate BD-OP0 state, as illustrated in Fig. 3(c). This suggests the existence of a convex free energy surface centering at OP theta 0°. On closer inspection, the spin configuration of this intermediate state is composed of two identical sub-lattices with even-L, which is formed by introducing two topological dislocations, in row and column, into the odd-L lattice. To minimize the size of dislocation and meanwhile to maximize the size of even-L sub-lattice, there are two different forms of the row dislocation depending on the specific odd-L value. For $L = 4n + 1$ ($n = 1, 2, ...$), an FM line dislocation is formed; for $L = 4n + 3$, an elongated OP0 at $L = 3$ is inserted as dislocation. The constructional difference leads to a difference in the topology, and hence the flattening process, of the convex free energy surface in response to the L increase. This is reflected by the difference in dynamics of this intermediate state as in the inset of Fig. 3(b), where its durations, quantified in the relaxation time position of the dip in the OP0.01 dynamics, at various L's are extracted and found to follow two distinct paths.

Different from the even-L case, the existence of the intrinsic 90(0)°-axis OP symmetry simplifies the picture of the L-dependent evolution of the free energy surface for the odd-L lattice (Fig. 3(d)). A similar process of the global loss of surface gradient is indicated by Fig. 3(e). Interestingly, the $(4n + 1) - (4n + 3)$ difference doesn't show up in the energy of the intermediate BD-OP0 state, reflecting again the topological nature of this difference only for the proximity of OP theta 0°. Though we can see clearly the different OP symmetry governs

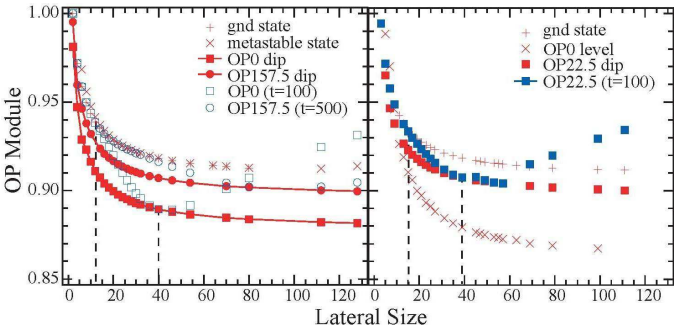


FIG. 4: (color) L-dependent OP modules of various states and OP module samplings at given relaxation times for (a) even-L, (b) odd-L. Note the vertical dash lines divide each of the $t = 100$ curves into three characteristic regions.

the whole spin dynamics evolution on the two kinds of lattices by means of the formation of a limited number of meta-stable/intermediate states (with concave/convex free energy surface, respectively) falling on the OP symmetry axes, the similarity in large-L evolution, combined with the gradual recovery of a non-intrinsic 0(90)°-axis OP symmetry in the even-L case, point to the unification in the extreme behavior at $L \to \infty$ when the even- and odd-L lattice become practically indistinguishable.

However, if the system is allowed to relax onto its final state, though through a sufficiently long time at large L to complete its boundary relaxation (insets of Fig. 2(b) and 3(b)), the difference in $|OP|$ of these BD states will NOT be smeared out for both kinds of lattice as suggested by the parallel saturations as seen for BD-OP135(45), BD-OP0 and BD-OP157.5 on even-L lattices (Fig. 4(a)), BD-OP45, BD-22.5 and intermediate BD-OP0 (Fig. 4(b)). Experimentally, the determination of the final state is restricted by the accessible observation time. In Fig. 4, examples are shown for both kinds of lattices, a non-monotonous behavior is expected in $|OP|$ sampled after a fixed relaxation time. For the initial states other than those on the OP symmetry axes, three well-defined regions are present depending on the comparison of the sampling time with the boundary relaxation time and saturation time. At the extreme case, where L goes to infinite and the even-odd difference naturally disappears, the boundary relaxation of the given homogenous PBC state seems indiscernible within any accessible experimental observation time, and thus, practically, the PBC-predicted continuously degenerate state is regarded to be stable.

This work was supported by the National Natural Science Foundation of China, the Cheung Kong Program, the Hong Kong Qiushi Science Foundation, and the Y. D. Fok Education Foundation.

[1] G. A. Prinz, Science **282**, 1660 (1998); M. Johnson, IEEE Spectrum **37**, 33 (2000); S. P. Li *et al.*, Nature **415**, 600 (2002).

[2] C. A. Ross *et al.*, J. Appl. Phys. **91**, 6848 (2002).

[3] Y. B. Xu *et al.*, IEEE Trans. Magn. **37**, 2055 (2001).

[4] Here $\Omega = (g\mu_B)^2$, g is the Lande factor, μ_B the Bohr magnetron.

[5] A. B. MacIsaac *et al.*, Phys. Rev. Lett. **77**, 739 (2002).

[6] D. S. Deng, X. F. Jin and R. B. Tao *et al.*, Phys. Rev. B **65**, 132406 (1996).

[7] A. Morello *et al.*, Phys. Rev. Lett. **90**, 017206 (2003).

[8] S. T. Bramwell, M. J. P. Gingras, Nature **294**, 1495 (2001).

[9] K. De'Bell *et al.*, Phys. Rev. B **55**, 15108 (1997) and references therein.

[10] H. Benson and D. L. Mills, Phys. Rev. **178**, 839 (1969). (***more to be cited here***)

[11] E. Rastelli *et al.*, Phys. Rev. B **66**, 054431 (2002); E. Rastelli *et al.*, *ibid.* **67**, 094429 (2003).

[12] See for example, William H. Press *et al.*, *Numerical Recipes in Fortran 77: The Art of Scientific Computing*, Chap. 12 , Vol. **1** of Fortran Numerical Recipes (University of Cambridge, Cambridge, 1996).

[13] M. Krech *et al.*, Comput. Phys. Commun. **111**, 1 (1998).

[14] For example, for the IP-AFM states, the equivalents for OP22.5 include OP67.5, OP202.5 and OP247.5 in even-L lattices, and additionally include OP112.5, OP157.5, OP292.5 and OP337.5. The equivalents share the same energy, OP module and all dynamical details. For completeness, the denotations in text should include the OP symmetry consideration.

[15] See reviews on cluster physics, W. A. de Heer, Rev. Mod. Phys. **65**, 611 (1993) and M. Brack, *ibid.* **65**, 677 (1993). (***more to be cited here***)

[16] The imaginary 3D free energy surface is the result of the combined evolution of unit energy and OP theta. We named in text the OP theta the x-axis (transverse), relaxation time the y-axis (longitudinal).